Electronic Supplementary Information

Hybrid nanocapsules for *in situ* TEM imaging of gas evolution reactions in confined liquids

Sardar B. Alam,[ab] Jiwoong Yang,[bc] Karen C. Bustillo,[a] Colin Ophus,[a] Peter Ercius,[a] Haimei Zheng[bd] and Emory M. Chan*[a]*

[a] The Molecular Foundry, Lawrence Berkeley National Laboratory, Berkeley, CA 94720, United States
[b] Materials Sciences Division, Lawrence Berkeley National Laboratory, Berkeley, CA 94720, United States
[c] Present Address: Department of Energy Science and Engineering, Daegu Gyeongbuk Institute of Science and Technology, Daegu 72988, Republic of Korea
[d] Department of Materials Science and Engineering, University of California, Berkeley, CA 94720, United States

* Email: emchan@lbl.gov, hmzheng@lbl.gov

Table of Contents

1. Captions for supporting movies

Movie S1. Formation and dynamics of nanobubbles in the interior of eight nanocapsules. The movie was recorded on a Ceta CMOS camera at 9.5 fps and 2048-pixel resolution in a Thermo Scientific Themis TEM at 300 kV. Total number of frames analysed for the data are 8127. The movie has been reduced in size by binning to 512 x 512 pixels, and five frames have been averaged, reducing the number of frames accordingly. The number of averaged frames was further reduced by factor of three (dropping the frames), resulting in a 15-fold reduction from the original frame number. Finally, the frames were cropped to minimize file size. Horizontal field width is 202 nm, and the frame playback rate has been increased 31.4-fold.

Movie S2. Gas transport from left nanocapsule to the right nanocapsule after they are fused. The movie was recorded at 5 fps and 512-pixel resolution in a JEOL 2100 TEM at 200 kV. The movie has been reduced in frames by factor of 2 by removing frames and cropped to minimize size. Horizontal field width is 104 nm, and the frame rate has been increased 12-fold.

Movie S3. Transport of gas between liposomes upon nanocapsule fusion. Only a fraction of the gas is transported to the receiving liposome as its volume is completely utilized, thus leaving a small bubble in the source liposome on the left. Movie frame rate increased 10-fold.

Movie S4. Growth and movement of a bubble in a nanocapsule. The liposome diameter increases as the bubble grows. The corresponding data is presented in Figure S14. The original movie was recorded at 512 x 512 pixels at 2 fps in a JEOL 2100 TEM at 200 kV. The movie has been reduced in frames by factor of 6 by removing frames, and the frame rate has been increased ~45-fold.

Movie S5. Transport of gas between two nanocapsules upon membrane fusion. The gas is transported from the smaller bubble to the larger bubble. Movie playback is 15.7 times faster than actual rate. Data is presented in Figure S17.

Movie S6. Growth and movement of a bubble in a nanocapsule. The corresponding data is presented in Figure S15. Movie playback is 6x faster than actual rate.

2. Methods

Liposome nanocapsule preparation: The bilayers of the liposomes used in this work were composed of POPC (1-palmitoyl-2-oleoyl-sn-glycero-3-phosphocholine) and cholesterol at 80:20 mole ratio. The liposomes were prepared using the well-established dry lipid film method[1]. POPC suspended in chloroform at concertation of 25 mg/ml was procured from Avanti Polar Lipids. In a 20 ml vial, 150 µl of POPC suspension was mixed with 95 µl of 5 mg/ml cholesterol which is also suspended in chloroform. The chloroform was evaporated from the solution by nitrogen stream while tilting and gently rotating the vial. This formed a dry lipid/cholesterol film around the walls of the 20 ml vial. The lipid film was further dried in a vacuum desiccator for 2 hrs. The film was rehydrated in 500 µl neat water, or an aqueous solution of 0.1 to 0.5 mg/ml chloroauric acid ($HAuCl_4$) in case of the Au-coated liposomes. The concentration of lipids in the final solution was 7.5 mg/ml. After rehydration, the solution was incubated at room temperature for two hours under gentle mixing with a magnetic stir bar. The size of the liposomes was controlled by passing the liposomes through a polycarbonate film with 50 nm holes (Avanti). 11 passes through the extruder results in an average liposome size of 55 nm. The size was verified by dynamic light scattering (DLS) with Wyatt DynaPro Plate Reader II (Figures S1).

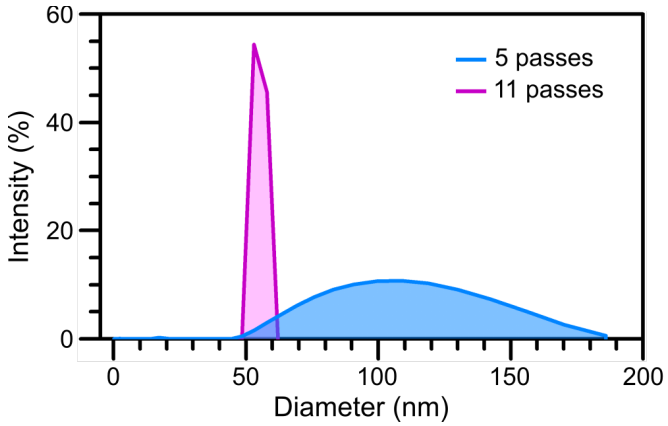

Figure S1. Diameter distribution of nanocapsules measured *ex situ* by dynamic light scattering. By extruding the liposome solution through a polycarbonate membrane with 50 nm pores the size distribution of the liposomes can be controlled. Eleven passes through the membrane delivers a monodispersed distribution of ca. 50 nm small liposomes.

Graphene liquid cell preparation: We prepared graphene liquid cells using graphene-transferred TEM grids.[2,3] Briefly, we transferred multilayer graphene (~6 layers, ACS material, US) onto Quantifoil carbon film TEM grids (Ted Pella Inc., US) by the direct transfer method. The liquid sample (< 0.5 µL) was dropped onto a graphene sheet supported on a TEM grids. This grid was covered with a second graphene-supported TEM grid, sandwiching the liquid between the two graphene sheets. The excess amount of solvent was removed by filter paper and the liquid

cells were compressed on the edges of the grids by tweezers for one hour. This promotes strong van der Waals interactions between two graphene sheets, which finally leads to the successful liquid encapsulation in graphene liquid cells**.** We first attempted to image liposome/water suspensions in graphene liquid cells to maximize contrast while limiting electron dose. We observed few liposomes with high resolution (Figure S2, S3). The hydrophobic graphene surfaces may disrupt the lipid bilayers, especially when compressed by the strong van der Waals forces that seal the graphene cells.

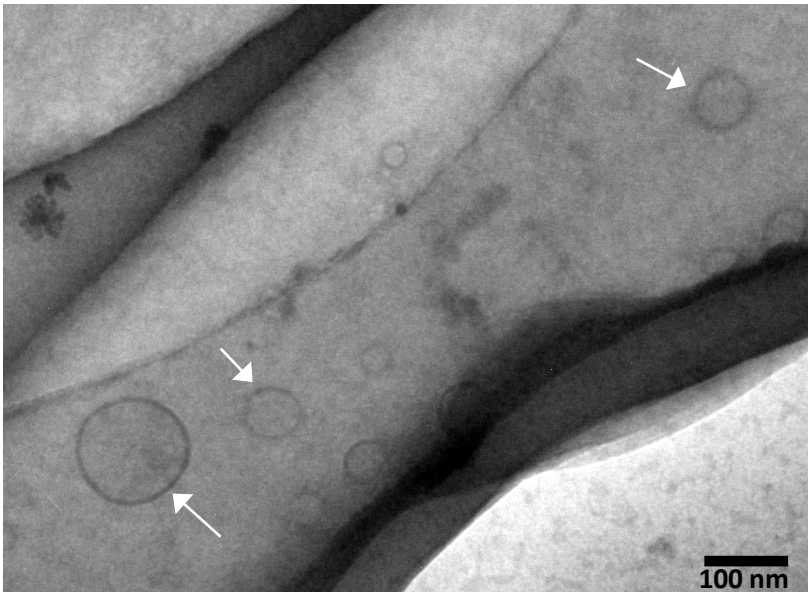

Figure S2. Multiple POPC liposomes encapsulated in graphene liquid cell. This was the highest number of liposomes recorded in a single image in the graphene liquid cell.

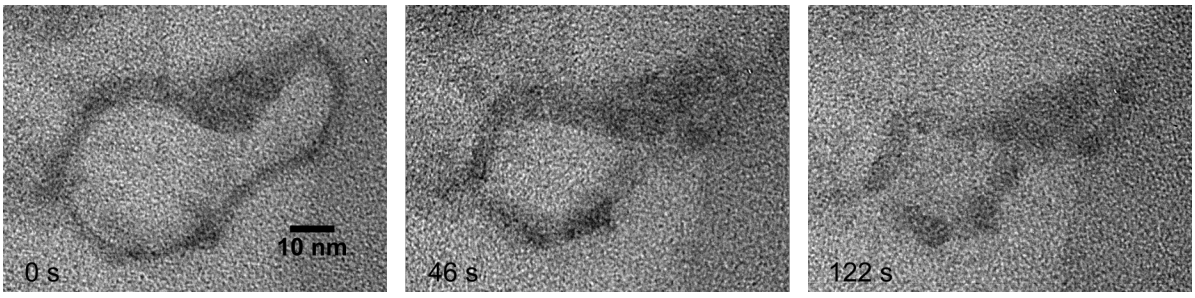

Figure S3: Liposome without the Au atoms coating in a graphene liquid cell denaturing on exposure to e-beam with a dose rate of ~250 $e^-/Å^2s$. The liposome was imaged in a JEOL 3010 TEM at 300 kV.

Carbon liquid cell preparation: As shown schematically in Figure S4, the carbon liquid cell was made by sandwiching thin layer of liposome sample between two 3 mm TEM grids with 10 nm amorphous carbon support film (Model CFLF400-CU-TH by Electron Microscopy Sciences). A volume of 2.5 µl is dispensed on one TEM grid and left for five minutes. This is followed by wicking most of the sample away from the grid with filter paper and placing a second TEM grid on top thus creating a sandwiched structure which encapsulates thin pockets of liquid sample. This TEM grid sandwich is held in place from the edge by self-closing tweezers for 10 to 15 minutes. The carbon liquid cell is then loaded in a vacuum leak check setup and, if it passes, transferred to the TEM. The encapsulation of lipid vesicles in carbon liquid cells is not a trivial problem as optimized surface conditions are required to avoid vesicle denaturing. The number of observable liposomes increased considerably (Figure S7, S8) when the grids were made hydrophilic before sample loading by ultraviolet ozone (UVO) cleaning for 45 s in Jelight Model 42 UVO-Cleaner. It takes less than 30 minutes to assemble and transfer cells to the TEM.

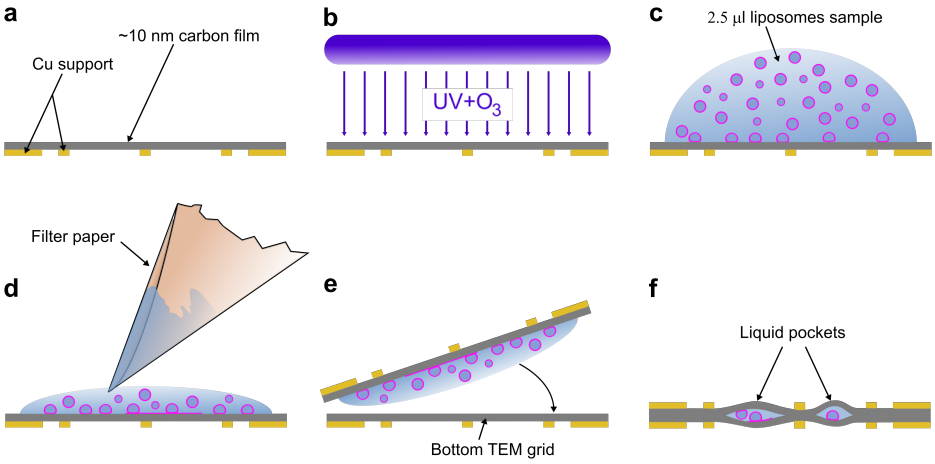

Figure S4. Schematic of carbon liquid cell preparation. **(a)** To make the liquid cells, we use commercially available 3 mm circular TEM grids with ca. 10 nm thin carbon film supported on a copper mesh. **(b)** The grids are treated with ultraviolet ozone cleaning for 45 s, followed by **(c)** dispensing 2.5 µl of sample containing liposomes. The sample drop that covers almost entire surface of the carbon grid is left for five minutes. **(d)** Afterwards, most of the liquid is wicked away from the grid with the tip of a piece of folded filter paper to leave a thin layer of liposome sample on the grid. **(e)** Finally, the grid with the thin liquid layer is placed on top of a second similar grid (also UVO cleaned) to create **(f)** a sandwiched structure with encapsulated liquid. This sandwich structure is held together from the edge by self-closing tweezers for 10 to 15 minutes.

TEM and image analysis: We used three TEMs for *in situ* experiments. Most experiments were conducted with a Thermo Scientific (formerly FEI) Themis 60-300 STEM/TEM operating at 300 kV in TEM mode and with electron dose in the range of 50 to 2000 $e^-/Å^2s$. The Thermo Scientific Themis has an image aberration corrector with spatial resolution down to 70 pm and Ceta 2 CMOS camera which we used to record movies at 2k x 2k size and 9.5 frames per second.

Experiments were also conducted using JEOL 2100 TEM at 200 kV JEOL 3010 TEM at 300 kV recording at 2 and 5 frames per second. The images were analyzed by segmenting bubbles from the recorded movies using a combination of in-house Matlab code and FIJI/Image J software.[4] Briefly, we (i) reduce the video resolution by binning to 512 x 512 or 256 x 256 pixels, (ii) homogenize the illumination across the frame, (iv) correct the drift, (v) apply median and band pass filter to enhance the contrast of features in the video, (vi) apply a threshold to isolate the bubble and convert the image to a binary format, (vii) fit an elliptical shape to the binarized feature of the bubble. In all analyses, the time $t = 0$ s marks the point when imaging in TEM starts. If the contrast was too low between the moving bubble and the surround water, we used Weka machine learning tool[5] in FIJI (Figure S5b) where 10 to 15 filtered images were used as training set to create probability maps for the entire video. The probability maps are subsequently binarized by selecting a threshold value that isolates the bubble. Finally, the ellipse is fit to the binarized bubble feature.

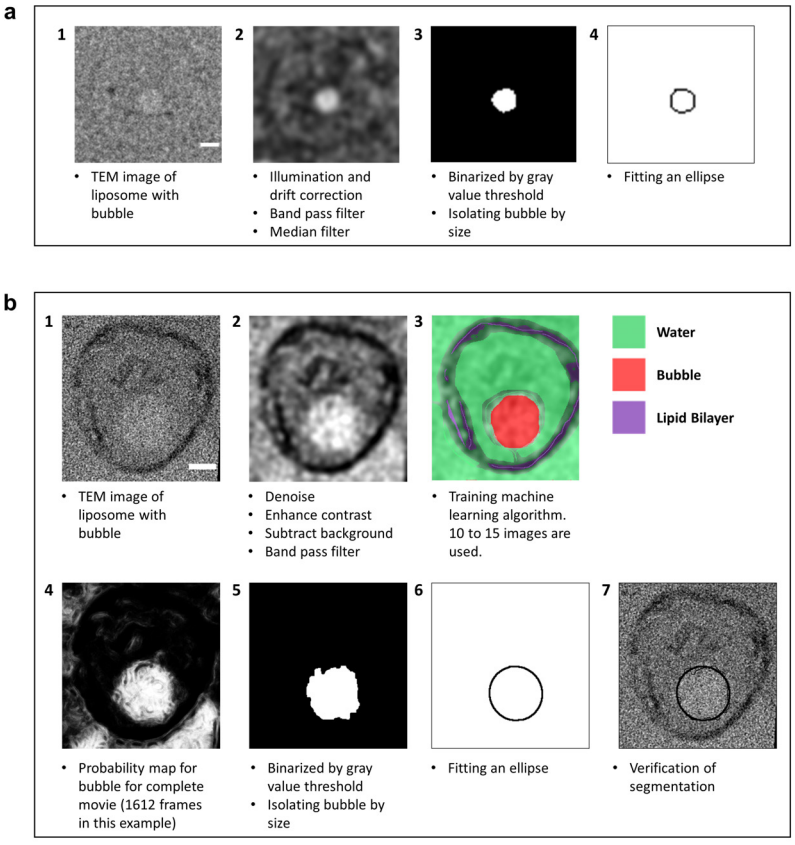

Figure S5. Image processing for segmenting bubbles. **(a)** When sufficient contrast exists between bubble and surrounding, we use filtering and threshold to segment the bubbles from the images. **(b)** When the contrast between bubbles and water is very low, we use Weka machine learning segmentation plugin in Fiji image processing tool. The stages in images processing are shown for both (a) and (b), where the scale bar is 10 nm.

3. Supplemental figures to complement main text figures

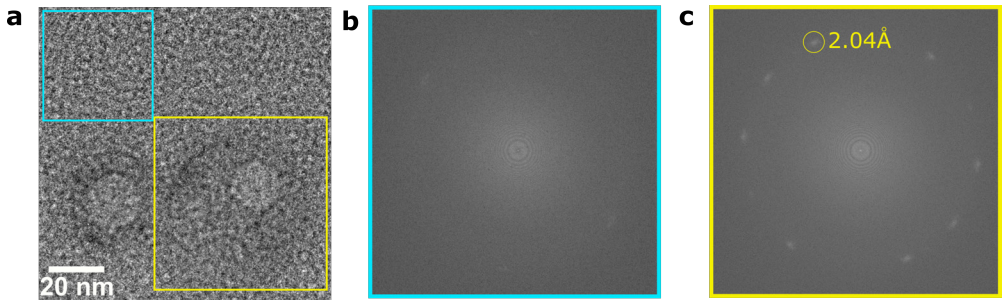

Figure S6. (a) TEM image of two Au coated liposomes with nanobubbles in their interior. These are the same liposomes shown in Figure 1d but recorded 8 minutes earlier at large negative defocus value. **(b)** and **(c)** FFT images for the regions marked in (a). For the region over the liposome, 2.04 Å reflections for the Au lattice spacing for (200) planes are visible.

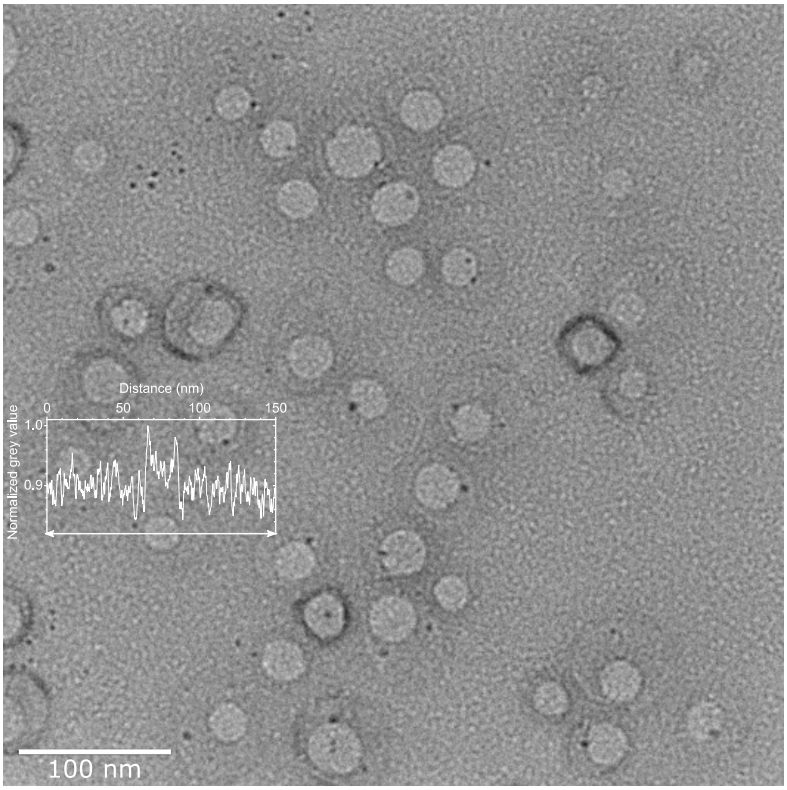

Figure S7. Multiple liposomes in viewing field, TEM image of liposomes with nanobubbles in a 513 x 513 nm^2 area encapsulated in amorphous carbon grid. A line profile of normalized gray values is plotted across a liposome with a bubble in its interior. The bubble interior has higher gray value while the aqueous interior of the liposome and its surrounding have similar gray values indicating the possible presence of water outside the liposomes. Dark spots, 3 to 7 nm in diameter, are gold nanoparticles that have nucleated from the Au source under the electron beam.

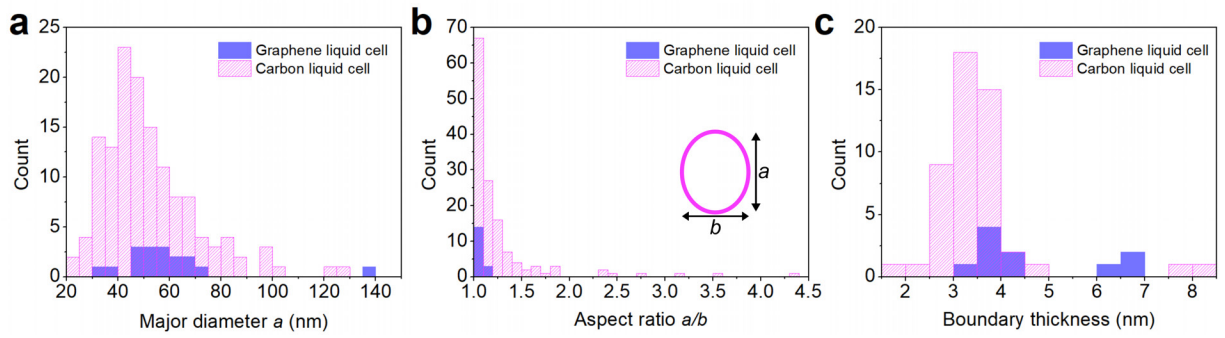

Figure S8. Size and shape of nanocapsules recorded with LCTEM. Histograms indicating the distribution of **(a)** diameter, **(b)** aspect ratio, and **(c)** shell thickness of the nanocapsules. Inside the TEM, majority of the nanocapsule are about 50 nm in diameter (as they are extruded through a membrane with 50 nm pores) and mostly circular with boundaries that are 2.5 to 4 nm thin.

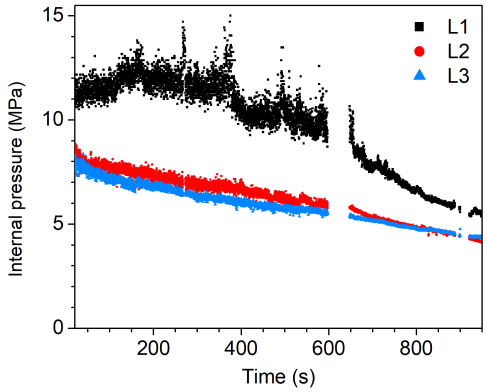

Figure S9. Internal pressure of nanobubbles in liposomes L1, L2 and L3 shown in Figure 2a.

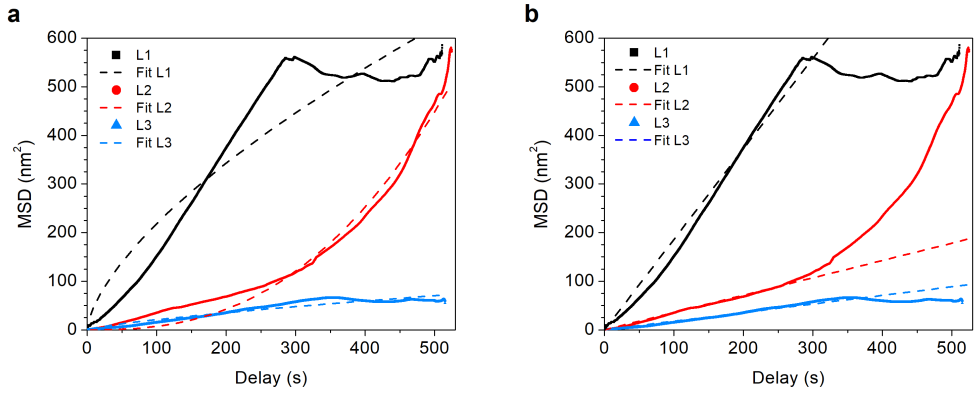

Figure S10. (a) Power law and **(b)** linear fits for the MSD plots[6] in Figure 4c. For fitting the linear model, delay times were only considered where the graph shows an approximately linear trend.

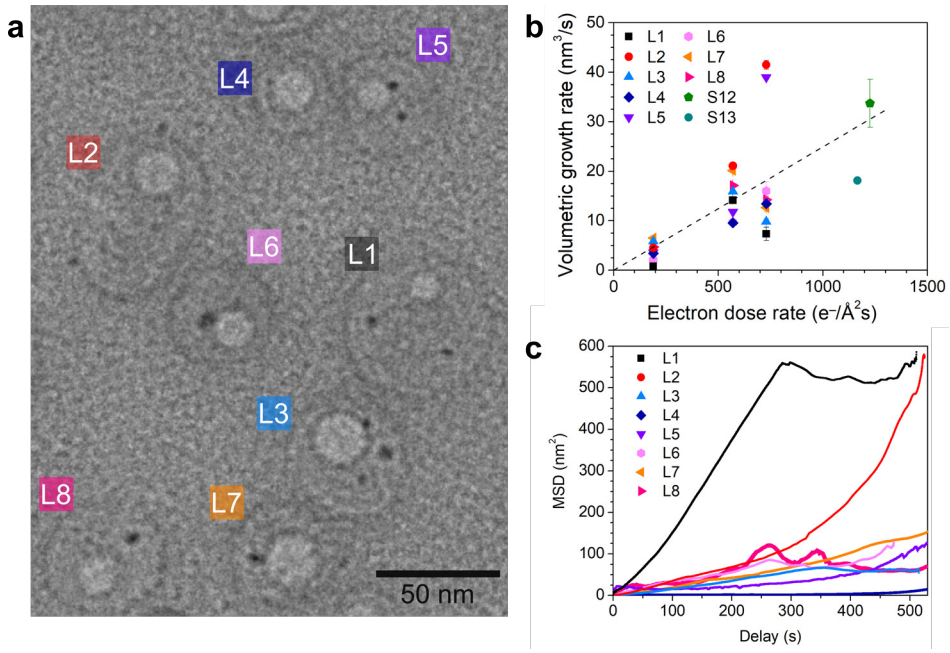

Figure S11. (a) Figure 2(a) reproduced with labelling for all eight nanocapsules. **(b)** Volumetric growth rate of bubbles plotted against electron dose for nanocapsules L1 to L8 in (a) and nanocapsules in Figure S12 and S13. **(c)** MSD plots for the bubbles in the eight nanocapsules in (a). MSD is only measured for the constant electron dose rate of 190 $e^-/Å^2s$.

4. Additional examples of bubbles in nanocapsules

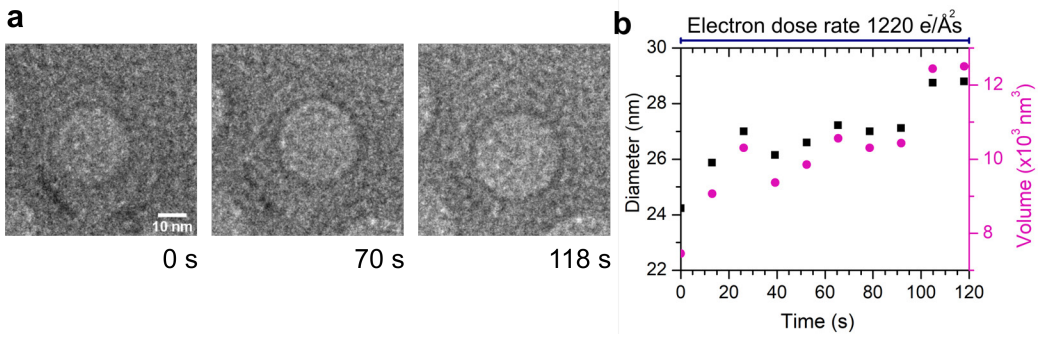

Figure S12. (a) TEM image sequence of bubble growing in liposome interior. The electron dose driving the bubble growth by radiolysis of water is 1220 $e^-/Å^2s$. (b) Diameter and volume of the bubble increases with time.

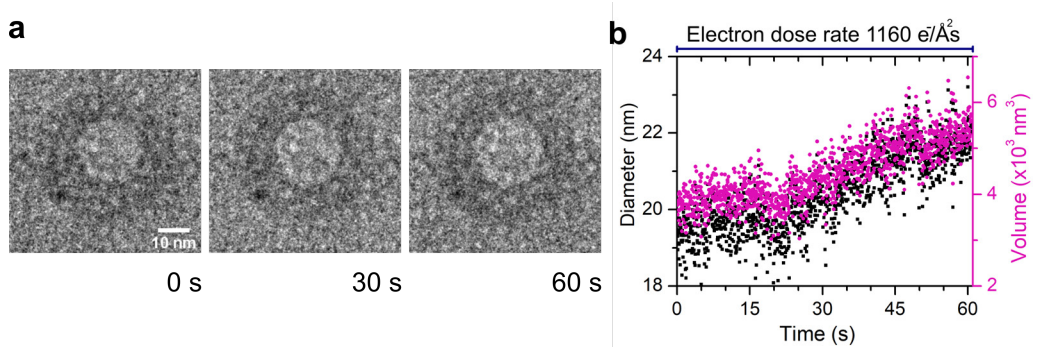

Figure S13. (a) TEM image sequence of bubble growing in liposome interior. The electron dose driving the bubble growth by radiolysis of water is 1160 $e^-/Å^2s$. **(b)** Diameter and volume of the bubble plotted against time.

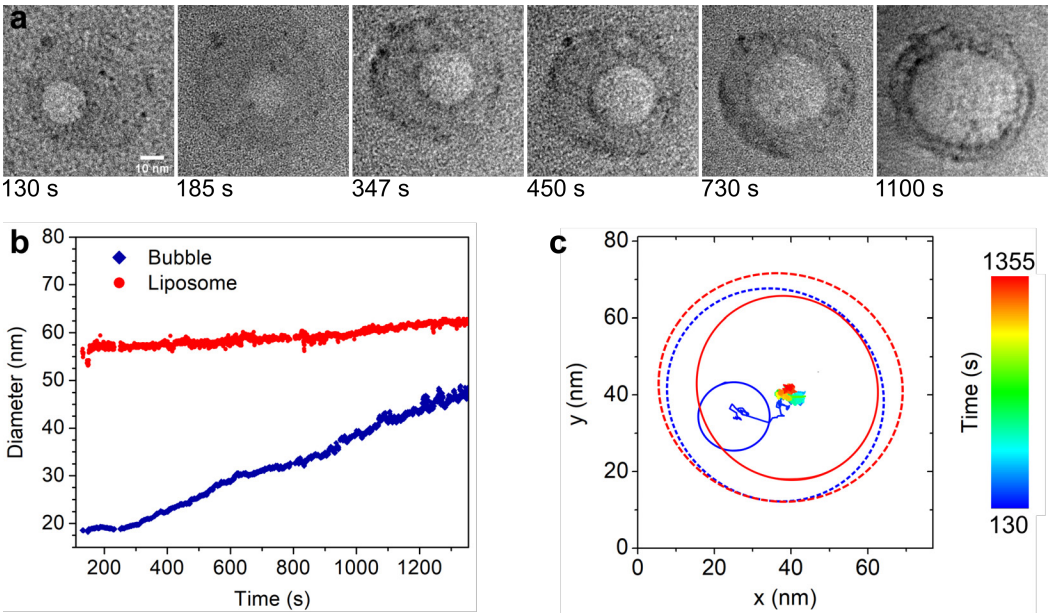

Figure S14. Case study in which a nanobubble occupies a large portion of the liposome volume. (a) TEM image sequence of bubble moving and growing in liposome interior. **(b)** The increase in the diameter of bubble and liposome with time. At 1355 s, the bubble diameter has grown to 47 nm. There is also increase in the size of the liposomes from ~ 57 nm at 200 s to 62 nm at 1355 s. **(c)** Trajectory of the bubble plotted with time. The solid ellipses indicate the bubble whereas dashed ellipses indicate the liposome boundary. The nanocapsule boundary was tracked using an in-house MATLAB code.

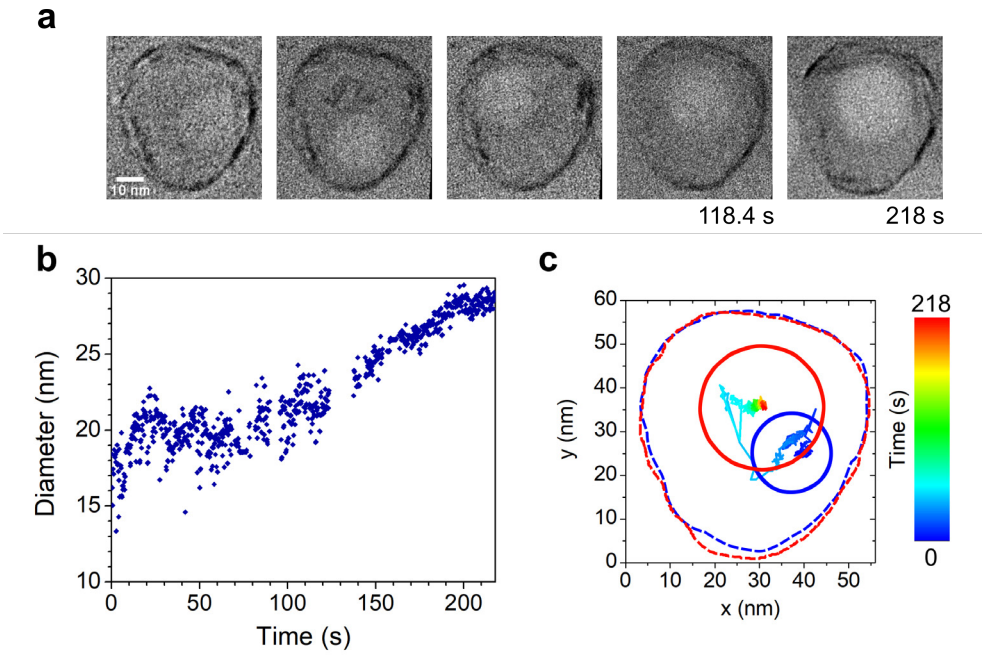

Figure S15. (a) TEM image sequence of bubble moving and growing in liposome interior. **(b)** The increase in the diameter of bubble with time. **(c)** Trajectory of the bubble plotted with time. The solid ellipses indicate the bubble whereas dashed ellipses indicate the liposome boundary. The video was analysed using Weka machine learning tool in FIJI image processing tool.[5]

5. Additional examples of gas transport between nanocapsules initiated by fusion

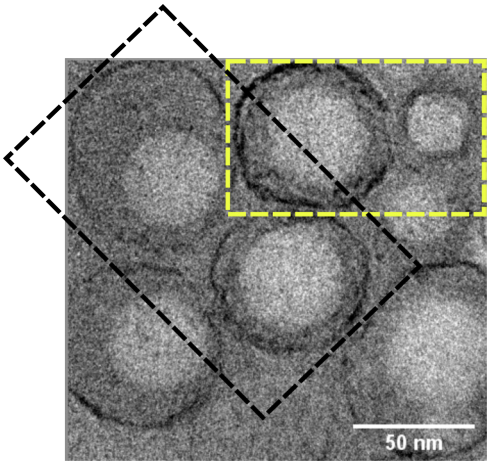

Figure S16. TEM image of multiple liposomes with gas bubbles. We observed gas transport between the pair of liposomes marked in black and yellow rectangles and presented in Figure 5c of main text and Figure S17, respectively. The images are recorded using a JEOL 2100 TEM operating at 200 kV.

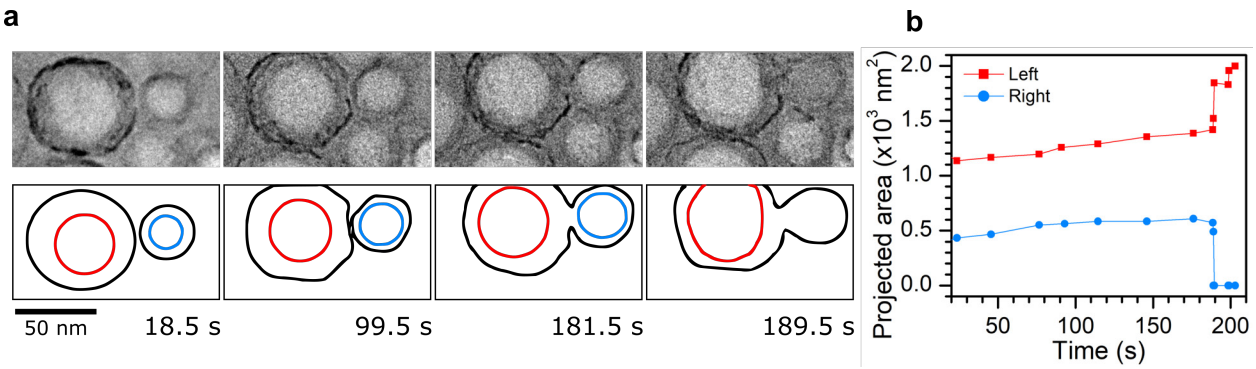

Figure S17. (a) TEM images and contour plot showing gas transport between liposomes initiated by fusion. Gas is transported from the smaller liposome (right) into the larger sized liposome (left). **(b)** Project area of bubbles in the left and right liposomes by 189.5 s, all gas from the left liposome is transferred to the right liposome. See full sequence in Supporting Movie S5.

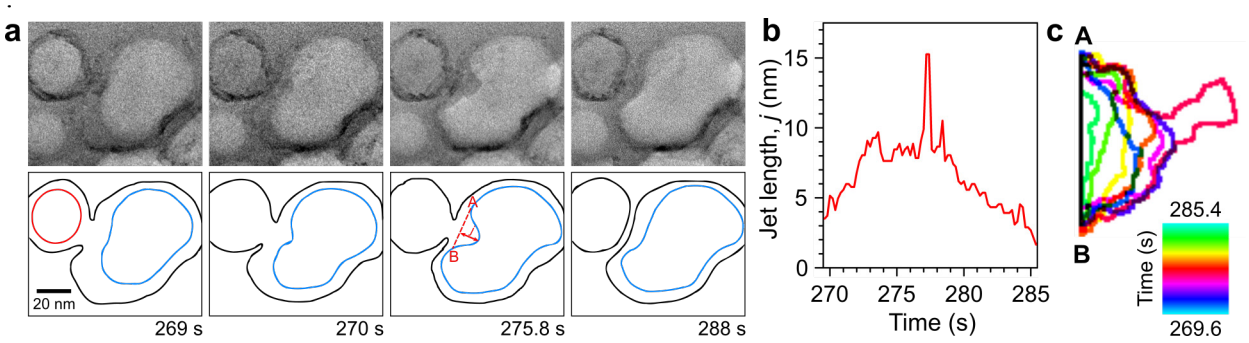

Figure S18. Liquid jet formation during gas transport from a smaller to larger liposome upon liposome fusion in Figure 5a shown with (a) additional frames and corresponding contours. (b) The length j and (c) the shape of the fluid jet formed at 275.8 s during gas transport from the smaller vesicle to the larger vesicle, also deforming the bubble. The direction and origin of j is shown with reference to the line AB marked in (a) at 275.8 s. The momentum of the jet, which has a liner velocity of ca. 1 nm/s, deforms the bubble for several seconds. See full sequence in Supporting Movie S2.

6. Stability, shape and transport of nanobubbles in liposomes

The high Laplace pressures induced by the small size of the nanobubbles (ca. 120 atm for a 10 nm bubble, Figure S9) in principle should favor their shrinking and dissolution. We tested the stability of the bubbles in the absence of gas generation by blanking the e-beam after initial nanobubble formation for 5 to 15 minutes. For example, in Figure S19, after nearly five minutes without electron exposure (from 438.4 to 735.6 s), we observed that the bubbles maintained their size. The stability and growth of nanobubbles in the absence of the e-beam suggests that the nanobubbles are larger than their critical radius and spontaneously grow due to the supersaturation of the surrounding fluid. On recommencing TEM imaging, we observed immediate gas transport as the gas from bubble B moves to C between two frames (735.6 s and 735.7 s). The gas in bubble A however transports via condensation-transmission-evaporation mechanism[7] meaning the transport is not immediate but takes time as seen in frames from 751.5 to 762.2 s.

Based on their movement (e.g., Figure 4b) we believe that the bubbles in the early stages are likely spherical in geometry and only loosely interacting nanocapsule walls. Since these nanobubbles are not tightly adhered to a surface, we can justify assigning a spherical geometry to them in the early stages when there is sufficient space within the liposomes to accommodate a spherical bubble. We assume that the aspect ratio of the liposomes, for example, in Figure 2 is greater than 0.5 in accordance with previous studies of liposomes adsorbed on surfaces[8,9] and hence we assume that bubbles with diameters smaller than the radius of the liposomes are spherical for the calculations in Figure 3ab and Figure S11b. The overlapping of bubbles A and B in Figure S19 without merging due to contact further indicates that the liposomes are not

significantly compressed between two carbon membranes and there is space available in the liposomes for two bubble to exist without merging.

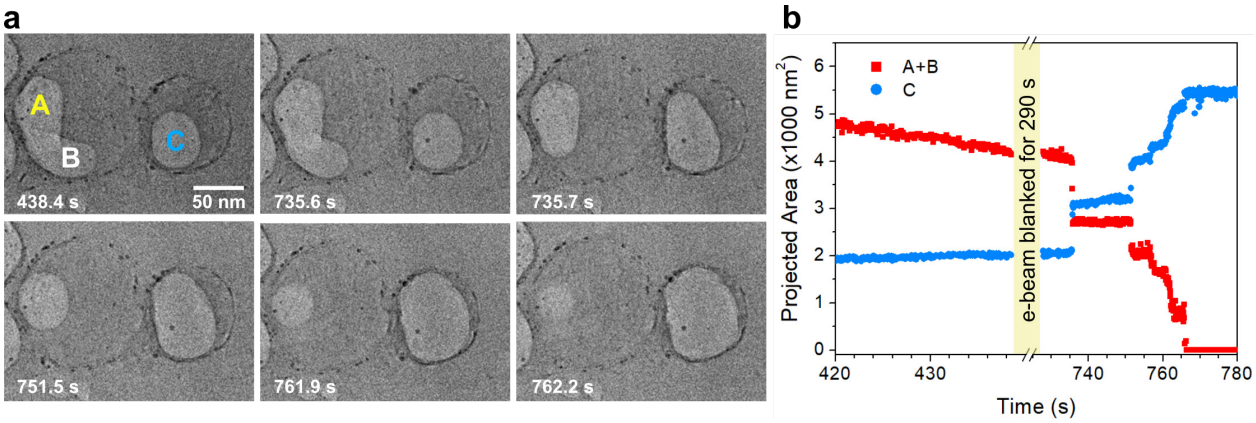

Figure S19. Stability of bubbles when e-beam is blocked and modes of bubble transport. **(a)** TEM images and **(b)** projected area showing the gas transport from bubbles A and B in left nanocapsules to bubble C in the right nanocapsule.

7. References

1 P. Walde and S. Ichikawa, *Biomol. Eng.*, 2001, **18**, 143–177.
2 J. M. Yuk, J. Park, P. Ercius, K. Kim, D. J. Hellebusch, M. F. Crommie, J. Y. Lee, A. Zettl and A. P. Alivisatos, *Science*, 2012, **336**, 61–64.
3 M. R. Hauwiller, J. C. Ondry and A. P. Alivisatos, *J. Vis. Exp. JoVE*, 2018, **135**, e57665.
4 C. T. Rueden, J. Schindelin, M. C. Hiner, B. E. DeZonia, A. E. Walter, E. T. Arena and K. W. Eliceiri, *BMC Bioinformatics*, 2017, **18**, 529.
5 I. Arganda-Carreras, V. Kaynig, C. Rueden, K. W. Eliceiri, J. Schindelin, A. Cardona and H. Sebastian Seung, *Bioinformatics*, 2017, **33**, 2424–2426.
6 N. Tarantino, J.-Y. Tinevez, E. F. Crowell, B. Boisson, R. Henriques, M. Mhlanga, F. Agou, A. Israël and E. Laplantine, *J Cell Biol*, 2014, **204**, 231–245.
7 D. Shin, J. B. Park, Y.-J. Kim, S. J. Kim, J. H. Kang, B. Lee, S.-P. Cho, B. H. Hong and K. S. Novoselov, *Nat. Commun.*, 2015, **6**, 6068.
8 K. Dimitrievski, *Langmuir*, 2010, **26**, 3008–3011.
9 E. Reimhult, F. Höök and B. Kasemo, *Langmuir*, 2003, **19**, 1681–1691.